Journal of Power Sources 262 (2014) 207–212

Contents lists available at ScienceDirect

Journal of Power Sources

journal homepage: www.elsevier.com/locate/jpowsour

# Infiltrated lanthanum strontium chromite anodes for solid oxide fuel cells: Structural and catalytic aspects

Tae-Sik Oh, Anthony S. Yu, Lawrence Adijanto, Raymond J. Gorte, John M. Vohs*

*Department of Chemical and Biomolecular Engineering, University of Pennsylvania, Philadelphia, PA 19104, USA*

## HIGHLIGHTS

- Infiltrated LSCr microstructure evolves in a significantly different way compared to infiltrated LSCM anode.
- Unfavorable microstructure of infiltrated LSCr limits its electrode performance.
- Exsolved metal nanoparticles from LSCr host lattice promote hydrogen electro-oxidation.
- Exsolved cobalt nanoparticles show low carbon deposition.

## ARTICLE INFO

*Article history:*
Received 29 December 2013
Received in revised form
27 March 2014
Accepted 28 March 2014
Available online 4 April 2014

*Keywords:*
Fuel cells
Catalyst
SOFC
Lanthanum strontium chromite

## ABSTRACT

Infiltration is a widely used fabrication method for solid oxide fuel cell (SOFC) composite electrodes. Here we report a study of the structure and electrocatalytic properties of SOFC anodes composed of a layer of lanthanum, strontium chromite ($La_{0.8}Sr_{0.2}CrO_3$, LSCr), both with and without added transition metal dopants, infiltrated into a porous yttria-stabilized zirconia (YSZ) matrix. The structural evolution of the electrode upon reduction and under typical SOFC operating conditions is compared to that reported previously for $La_{0.8}Sr_{0.2}Cr_{0.5}Mn_{0.5}O_3$–YSZ composite anodes. For the transition metal doped materials, a portion of the metal dopants were found to be exsolved from the LSCr lattice upon reduction and to be effective in promoting electro-oxidation of hydrogen. Exsolved cobalt particles were also found to be relatively stable when exposed to hydrocarbon fuels with low activity for the formation of carbon deposits.



## 1. Introduction

Electronically conductive ceramics have a number of features that make them attractive for use in solid oxide fuel cell (SOFC) anodes. Compared to present state-of-the-art anodes which use Ni as the electronically conductive phase, ceramic conductors are more tolerant of hydrocarbon fuels since they are less prone to deactivation via carbon deposition and can be redox stable [1–7]. In this regard, a particularly interesting mixed ionic/electronic conductive ceramic is (La,Sr)(Cr,Mn)$O_3$ (LSCM) [1]. Very good performance has been achieved for SOFC composite anodes that use LSCM that has been infiltrated into a pre-existing porous YSZ (yttria-stabilized zirconia) scaffold as the electronically conducting phase [2,3]. Since LSCM has low intrinsic catalytic activity a metal catalyst must also be added. The modest electronic conductivity of LSCM requires, however, that the electrode be relatively thin in order to maintain the ohmic loss at an acceptable level. For example, a porous YSZ slab infiltrated with 45 wt % $La_{0.8}Sr_{0.2}Cr_{0.5}Mn_{0.5}O_3$ has a conductivity of just 0.1 S $cm^{-1}$ at 973 K [2]. Ideally, one would like to have a composite conductivity of at least 1 S $cm^{-1}$ [4].

While low conductivity is an issue, LSCM–YSZ composites prepared by infiltration have a number of interesting features. Under the oxidizing conditions used during synthesis, the infiltrated LSCM forms a conformal film that completely covers the YSZ scaffold. In contrast, under reducing conditions that are typical of an operating anode, this film de-wets the YSZ forming a porous layer with a high degree of surface roughness, while still maintaining the connectivity within the LSCM perovskite phase [3,5]. As has been discussed previously, this produces an ideal structure for an SOFC anode with a high concentration of three-phase boundary (TPB) sites that are active for electro-oxidation

* Corresponding author. Tel.: +1 215 898 6318.
*E-mail address:* vohs@seas.upenn.edu (J.M. Vohs).

http://dx.doi.org/10.1016/j.jpowsour.2014.03.141
0378-7753/

of the fuel [3,5]. It is noteworthy that $La_{0.8}Sr_{0.2}MnO_3$ (LSM), the conventional cathode material, has also been observed to exhibit wetting of an YSZ scaffold under oxidizing conditions and then break into particles under lower oxygen pressures due to reduction of the Mn [6].

Because of its high conductivity, Sr-doped $LaCrO_3$ (LSCr) is another promising material for use as the electronically conducting phase in SOFC anodes. LSCr is widely used as an interconnect material [10] and has an electrical conductivity that is ~10 times greater than that of LSCM under reducing conditions (973 K, 10% $H_2/N_2$) [9]. It also has a well-known defect structure [11] and outstanding chemical stability. The high conductivity of LSCr would allow for thicker and more robust ceramic SOFC anodes while still maintaining an acceptably low ohmic resistance. It is not clear, however, if LSCr will have the same favorable interactions with YSZ as observed for LSCM which helped to produce structures with high TPB lengths. Since LSCr is hard to sinter [10] compared to LSCM, it may undergo a different microstructural evolution under oxidizing and reducing conditions. In order to assess the suitability of LSCr for the electronically conducting phase in SOFC anodes, in the present study we have characterized the electrical conductivity of porous LSCr/YSZ composites and how interactions at the LSCr–YSZ interface affect the microstructure of infiltrated LSCr films under both oxidizing and reducing conditions.

In addition to characterizing these physical properties of infiltrated LSCr/YSZ composite anodes, we also investigated methods to enhance their catalytic activity. As noted above, addition of a small amount of metal oxidation catalyst (<0.5 wt%) is generally required in order to obtain good performance with these types of oxide anodes [3,4,7]. For example, it has been shown that the addition of a Pd/ceria catalyst to an infiltrated LSCM/YSZ anode is sufficient to cause a 10-fold increase in the peak power density [3]. Similar behavior has been observed for SOFC anodes in which $La_{0.7}Sr_{0.3}VO_{3.85}$ [4] and $La_{0.3}Sr_{0.7}TiO_3$ [7] have been used as the electronically conductive phase. While the catalytic metals can be added using standard wet infiltration techniques, they can also be produced *in situ* via exsolution of dopant metal ions from an oxide host [12–17]. This phenomenon has been observed for a variety of perovskite oxides including lanthanum chromate doped with nickel, ruthenium, and palladium [12–14]. We, therefore, chose to investigate this approach for adding catalytic metal nanoparticles to the surface of LSCr/YSZ composite anodes. The specific system investigated was $La_{0.8}Sr_{0.2}Cr_{1-x}M_xO_3$ with M being Co, Cu, and Ni. The performance of SOFC with $La_{0.8}Sr_{0.2}Cr_{1-x}M_xO_3$/YSZ composite anodes are reported and demonstrate both exsolution of the metals and their enhancement of the catalytic activity and overall cell performance.

## 2. Experimental

Bulk powders of pure and transition-metal doped LSCr and LSCM were synthesized using aqueous solutions of $La(NO_3)_3\cdot 6H_2O$ (Alfa Aesar, 99.9%), $Sr(NO_3)_2$ (Alfa Aesar, 99%), $Cr(NO_3)_3\cdot 9H_2O$ (Alfa Aesar, 98.5%), $Co(NO_3)_2\cdot 6H_2O$, $Cu(NO_3)_2\cdot 3H_2O$, and $Ni(NO_3)_2\cdot 6H_2O$ (Alfa Aesar, 99.9%), and citric acid which was used as a chelating agent. The precursor solution with the desired ion concentrations was initially evaporated on a hot plate to form a gel which was then calcined in air at 1473 K to form the perovskite phase as confirmed by X-ray diffraction. Care was taken to avoid the formation of secondary phases, such as $SrCrO_4$ [18]. The A-site lanthanum to strontium ratio was held constant at four and a B-site doping level of the transition metals of 10 at% was used in all cases. For instance, the composition of the LSCr–Ni sample was $La_{0.8}Sr_{0.2}Cr_{0.9}Ni_{0.1}O_3$.

DC four-probe electrical conductivity measurement were performed using porous YSZ slabs (65–70% initial porosity) which were infiltrated with precursor metal nitrate solution in a repeated fashion, with heating from room temperature to 723 K after each infiltration and finally to higher temperature (1473 K for chromites) in order to form the perovskite phase. The process was continued until the mass of the perovskite phase accounted for 45% of the total mass. For an YSZ scaffold with 65% porosity, 45 wt% LSCr corresponds to filling 40% of the initial pore volume (39% final porosity). A similar level of final porosity is expected for the LSCM infiltrated slab. Silver paste (SPI Supplies, 5063-AB) and wires were used to make electrical contacts to the slabs and conductivity measurements were made with the slabs exposed to wet $H_2$ (3% $H_2O$) between 873 and 1073 K. These same slabs were also used for coke-resistance tests after removing the silver leads. For these measurements the slabs were first reduced in flowing dry $H_2$ for 4 h at 1073 K and then cooled to room temperature. After measuring their mass, they were heated in dry $H_2$ to 1073 K and then the gas phase was switched to flowing dry $CH_4$. After 1 h in the $CH_4$ the temperature was lowered while maintaining $CH_4$ flow. The final mass was then measured to determine the amount carbonaceous material deposited on the sample.

SOFC performance studies were done using YSZ electrolyte-supported button cells that were fabricated by laminating three green tapes followed by sintering in air (1773 K, 4 h) [19]. The outer two tapes contained sacrificial pore formers (synthetic graphite, 300 mesh, Alfa Aesar), so the resulting cell consisted of a porous (60 μm thick)-dense (75 μm)-porous (60 μm) layered YSZ structure. The structure and properties of the porous YSZ scaffolds formed in this manner have been reported previously [20–22]. LSCr or LSCM were added to the anode (45 wt% (42 vol%) of the anode composite) using the infiltration procedure described above, and a $La_{0.8}Sr_{0.2}FeO_3$ cathode (40 wt% (38 vol%) of the cathode composite) was formed in the same way, but using a lower calcination temperature of 1123 K [15]. All electrode composites had a final porosity close to 40% which was sufficient to insure that gas transport did not limit performance for the conditions used this study. For some cells Pd and/or $CeO_2$ were added to the anode by infiltration [3,4,7]. For Pd infiltration, palladium nitrate aqueous solution (Alfa Aesar, 99.9%) was used. For ceria, $Ce(NO_3)_3\cdot 6H_2O$ (Alfa Aesar, 99.5%) was dissolved in water. When both were added to an anode the ceria was added before the Pd. The cells were calcined in air at 723 K following the addition of these species.

The button cells were mounted and sealed onto an alumina tube using Aremco Ceramabond 552, and silver paste (SPI Supplies, 5063-AB) and wires were used for current collection. The typical thickness of applied silver layer was 0.5 mm. This layer is sufficiently porous such that it does not affect cell performance and high current densities have been achieved using this current collector [15]. The silver paste covered the entire surface of each electrode. This area (0.35 $cm^2$) was used for current density calculation. All electrochemical data were collected using a Gamry Instruments potentiostat with the cathode exposed to stagnant air while humidified $H_2$ (3%$H_2O$) was swept over the anode. Impedance spectra were recorded in the galvanostatic mode at open circuit for frequencies from 0.1 to 300 kHz using an AC amplitude of 1 mA. $V$–$i$ curves and impedance spectra were collected after heating in $H_2$ to the desired measurement temperature without any additional pretreatment.

To determine cell compositions and microstructures, X-ray diffraction patterns were collected with Cu Kα radiation in Bragg–Brentano geometry (Rigaku Hyperglex, 40 kV, 30 mA). Sometimes, a small amount of YSZ powder was mixed in as an internal reference. Rietveld refinement was carried out on YSZ-free diffraction patterns using the GSAS package [23] with EXPGUI interface [24]. SEM images were taken with a JEOL 7500F HRSEM operating with a 5 kV acceleration voltage.

## 3. Results and discussion

### 3.1. Characterization of LSCr samples

For the LSCr powder samples, XRD confirmed that the desired perovskite phase was formed following calcination in air for 4 h at 1473 K. The same calcination conditions were used to obtain phase-pure LSCM perovskite powders in our previous work [2]. Fig. 1(a) shows the intensity vs. $2\theta$ scan for as-calcined LSCr powder mixed with YSZ. Rietveld refinement determined the crystal is orthorhombic ($a = 5.450$ Å, $b = 7.756$ Å, $c = 5.495$ Å, $V = 232.3$ Å$^3$) with a unit cell volume very close to the reported value [18]. The XRD pattern obtained from an YSZ–LSCr powder mixture reduced for 4 h at 1073 K in dry hydrogen (Fig. 1(b)) shows that this treatment did not result in any significant reaction between the phases or phase decomposition. There is a small peak at 43°, however, indicating the presence of an unknown impurity phase. The XRD pattern of the anode side of a measurement-ready cell which was infiltrated with both LSCr and then $CeO_2$ is shown in Fig. 1(c) and also confirms that the LSCr perovskite phase was formed. Note that the impurity phase is not present in this sample.

### 3.2. Comparison of LSCr and LSCM

In the literature, the electrical conductivity of $La_{0.75}Sr_{0.25}CrO_3$ is reported to be about one order of magnitude higher than that of $La_{0.75}Sr_{0.25}Cr_{0.5}Mn_{0.5}O_3$ at 973 K in 10% $H_2/N_2$ [9]. As noted in the introduction, this was our primary motivation for using LSCr as the conducting phase in an SOFC anode. Consistent with the electrical conductivities, the data in Fig. 2 shows that the conductivity of a porous YSZ slab infiltrated with LSCr (1 S cm$^{-1}$ at 973 K) is also higher than that of LSCM-infiltrated YSZ (the LSCM data is from Ref. [2]). The difference in conductivity is about one order of magnitude, which is in good agreement with expected values based on the electrical conductivities of these materials. These data also show that in contrast to LSCM–YSZ, the conductivity of LSCr–YSZ decreases with increasing temperature. This has also been observed for $La_{0.8}Sr_{0.2}Cr_{0.95}Ni_{0.05}O_3$ under reducing conditions ($P_{O_2} \leq 10^{-15}$ atm, 1223–1273 K) [25]. For $LaCrO_3$ and $YCrO_3$, it is known that the dominant electronic charge carriers are localized holes at chromium sites [25,26]. The equilibrium extent of oxidation of the LSCr lattice increases (i.e. $Cr^{4+}$ concentration increases) as the temperature is lowered under reducing atmospheres leading to the conductivity increase. Interestingly, as shown in Fig. 2, doping copper on the chromium site lowers the total conductivity.

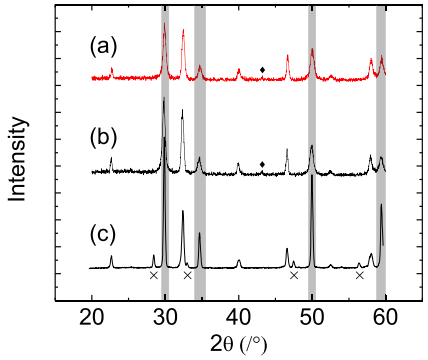


**Fig. 1.** XRD patterns of (a) YSZ–LSCr powder mixture before reduction, (b) YSZ–LSCr powder mixture after reduction (800 °C, 4 h in dry $H_2$), and (c) measurement-ready LSCr (45 wt%) infiltrated anode with ceria (5 wt%). "x" marks show ceria peak positions, and vertical shaded bands denote YSZ peaks. Diamond marks show an unknown peak at 43°.

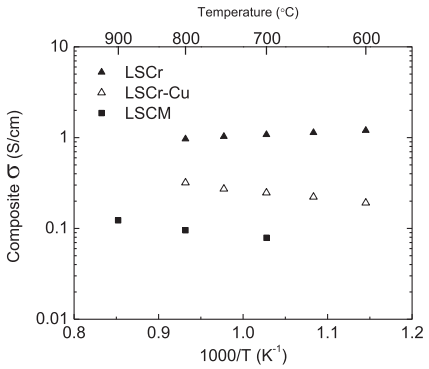


**Fig. 2.** Electrical conductivity of the 45 wt% perovskite–YSZ composite in humidified $H_2$ (3% $H_2O$) as a function of temperature.

This detrimental effect of copper has also been reported for $(La_{0.8}Ca_{0.2})(Cr_{0.9-x}Co_{0.1}Cu_x)O_3$ [27].

Somewhat surprisingly, the differences in the electrical conductivity of the LSCr–YSZ and LSCM–YSZ composites are not manifest in SOFC performance data obtained from the button cells operating on humidified $H_2$ fuel at 973 K, as shown in Fig. 3. (The polarization curve for LSCM is from Ref. [2].) Note that for these cells, $Pd/CeO_2$ was added to the anodes to enhance catalytic activity. These data show that despite the higher composite conductivity of LSCr-based anode, the cell with the LSCM-based anode considerably outperforms it. It is noteworthy that we have obtained similar results in a previous study comparing anodes which use $La_{0.3}Sr_{0.7}TiO_3$ and $La_{0.8}Sr_{0.2}Cr_{0.5}Mn_{0.5}O_3$ as the conducting phase, where the highest performance was again observed for the LSCM which has lower electrical conductivity [3]. Together these results suggest that other factors, such as structure and TPB length, play a critical, if not dominate, role in determining overall performance.

The importance of microstructure in anode performance is more apparent when one examines SEM images of the anodes, such as those displayed in Fig. 4 for porous LSCr–YSZ and LSCM–YSZ composites before and after reduction at 1073 K in wet $H_2$ (3% $H_2O$). The image of the unreduced LSCr–YSZ sample (panel a) shows that the infiltrated LSCr layer has a somewhat granular structure, but still forms an interconnected film on the surface of the porous YSZ scaffold. Upon reduction, however, the SEM image (panel b) shows

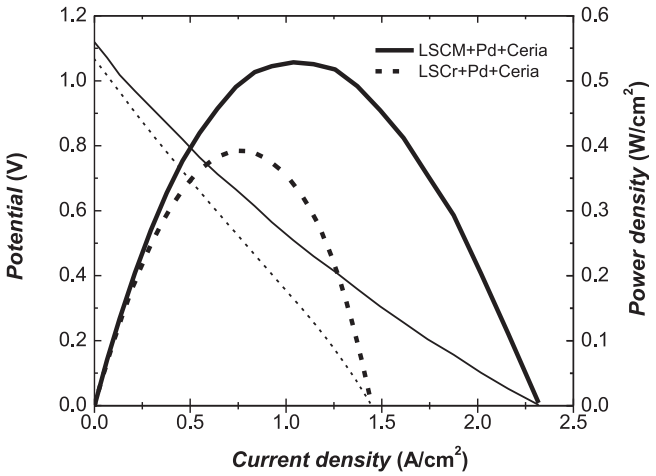


**Fig. 3.** *V–i* and *V*–power density polarization curves for cells with 45 wt% perovskite calcined at 1473 K, with 5 wt% ceria and 0.5 wt% Pd. Fuel condition: 973 K in humidified $H_2$ (3% $H_2O$). Cathodes were exposed to stagnant, ambient air. The thin and thick lines correspond to the voltage and power curves, respectively.

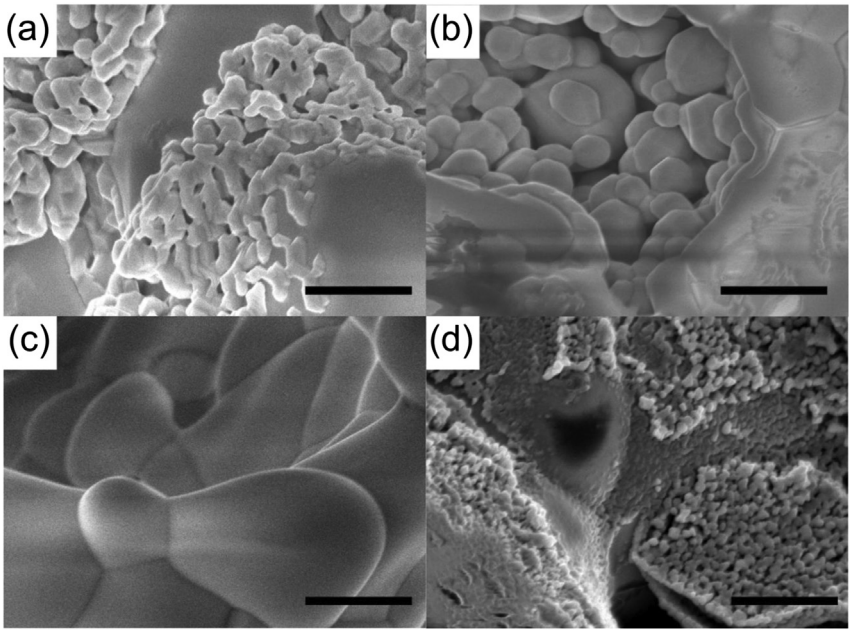


**Fig. 4.** SEM images of a YSZ porous scaffold infiltrated with either LSCr or LSCM. (a) LSCr before reduction, (b) LSCr after reduction, (c) LSCM before reduction, and (d) LSCM after reduction. The scale bars are for 1 μm.

that the LSCr film undergoes significant agglomeration resulting in both a decrease in surface area and the formation of isolated LSCr grains which are not electrochemically active. This behavior greatly differs from that of the LSCM–YSZ composite where, as reported previously [3,5], the LSCM forms an even coating on the YSZ under oxidizing conditions (panel *c*) which breaks into a highly porous interconnected film with fine grain structure upon reduction (panel d). These images vividly show that the degree of wetting of the perovskite phase on the YSZ is much less for LSCr compared to LSCM. The enhancement of the wetting of the YSZ surface upon addition of Mn has been discussed previously [6]. These images also clearly show that under reducing conditions that are typical of an operating SOFC anode, there is a much higher concentration of electrochemically active TPB sites for the LSCM–YSZ composite compared to the LSCr–YSZ composite.

The impedance spectra reported in Fig. 5 for cells with LSCr–YSZ composite anodes provides additional evidence for the inferior connectivity in the LSCr layer upon reduction. Cole–Cole impedance plots for cells in which Pd and Pd + $CeO_2$ have been added to the LSCr–YSZ composite anode to enhance catalytic activity are displayed in this figure. Note the drastic decrease in the non-ohmic impedance arising from the addition of ceria to the anode. The non-ohmic ASR goes from 1.33 to 0.39 Ω $cm^2$ upon ceria addition. While the $CeO_2$ may provide some enhancement of the catalytic activity of

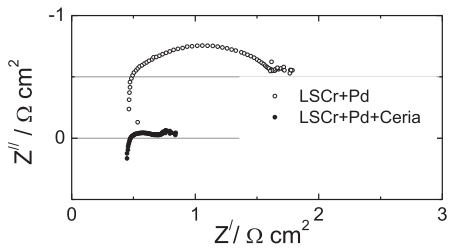


**Fig. 5.** Open circuit Cole–Cole plots for cells with 45 wt% LSCr calcined at 1473 K and (open circles) 0.5 wt% Pd or (closed circles) 0.5 wt% Pd plus 5 wt% $CeO_2$ added to enhance catalytic activity. Operating conditions: 973 K in humidified $H_2$ (3% $H_2O$). Cathodes were exposed to stagnant, ambient air.

the Pd, analogous previously reported results for the addition of Pd and Pd + $CeO_2$ to LSCM–YSZ composite anodes show this effect to be minimal [9]. These observations along with the fact that ceria is electronically conducing under reducing conditions, suggests that a more likely explanation is that the added $CeO_2$ provides conducting bridges between isolated LSCr particles, thereby increasing the active surface area of the anode. Thus, the combined SEM and impedance results provide strong evidence that the observed variations in anode microstructure are the likely origin of the differences in cell performance shown in Fig. 3.

### 3.3. Doping LSCr with catalytic transition metals

LSCr (and LSCM) has low catalytic activity and doping with a highly catalytic metal is required in order to obtain an anode with an acceptably low ASR. In the fuel cell tests presented in the previous section, the catalytic activity of the anode was enhanced by depositing a small quantity of Pd or Pd/$CeO_2$. As discussed in the introduction, catalytic metal particles can also be produced *in situ* by substituting a small fraction of the B sites in the LSCr with a catalytic metal, such as Ni or Co, which can be exsolved form the perovskite lattice under reducing conditions. This approach is demonstrated in Fig. 6 which presents polarization curves (humidified $H_2$ fuel, 973 K) for SOFCs using Cu-, Co-, and Ni-doped LSCr as the electronically conducting phase. Data for undoped LSCr is also included for comparison. Corresponding impedance spectra for each cell obtained at OCV are displayed in Fig. 7. In our previous work, the area specific resistance at 973 K of LSF/YSZ composite cathodes similar to those used here was found to be 0.15 Ω cm [28]. Thus, the impedance arcs are dominated by processes occurring on the anodes.

These data illustrate several important points. First, a portion of the transition metal appears to be exsolved from the perovskite lattice under the reducing conditions producing catalytically active metal nanoparticles that greatly enhance the overall cell performance and decrease the anode ASR. Second, there is a significant variation in the catalytic activity of the exsolved metal nanoparticles with Cu and Ni providing the smallest and largest

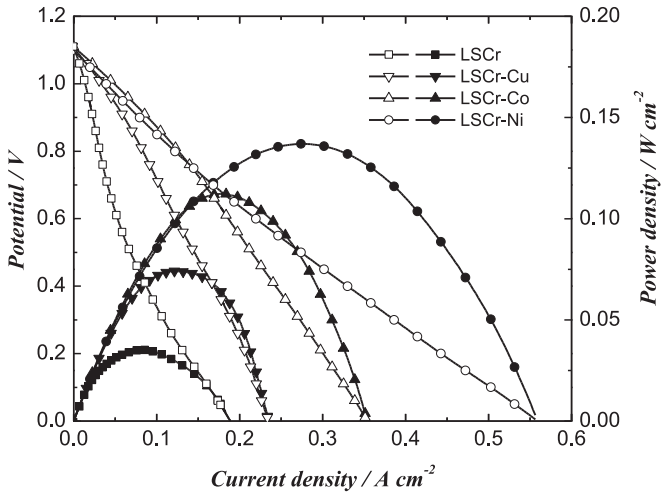


**Fig. 6.** *V*–*i* and *V*–power density curves for cells with 45 wt% transition-metal doped LSCr calcined at 1473 K. The transition metal dopants are indicated in the figure. Operating conditions: 973 K in humidified $H_2$ (3% $H_2O$). Cathodes were exposed to stagnant, ambient air. Open and closed symbols correspond to the voltage and power curves, respectively.

enhancements in overall performance, respectively. While Cu has the lowest catalytic activity of the metals studied and also decreases the overall conductivity of the LSCr, it is noteworthy that it still significantly increased overall performance.

Exsolution of a high fraction of the metal from the LSCr perovskite lattice might be expected to produce relatively large (>10 nm) metal particles that could be detected by XRD; however, peaks indicative of the metals (Cu, Co, and Ni) were not detected from samples that were reduced at 1173 K for 4 h in wet hydrogen. Thus, it appears that either only a small fraction of the transition metal on the B site was exsolved and/or the resulting metal particles were exceptionally small and not detectable by XRD. There is precedence for this in the literature. For example, Arrivé et al. were unable to detect exsolved Ni particles from reduced $La_{0.5}Sr_{0.5}Ti_{0.75}Ni_{0.25}O_3$ by XRD (1073 K, 48 h in 2% $H_2$/Ar), but were able to observe by TEM [29]. Thus, the fuel cell performance and XRD data obtained here suggest that for the conditions used in this study only a small amount of the B-Site transition metal was exsolved form the perovskite lattice upon reduction.

As noted in the introduction, high hydrocarbon stability is one advantage of using conducting perovskites as the electronically conducting phase in SOFC anodes. This advantage will be lost,

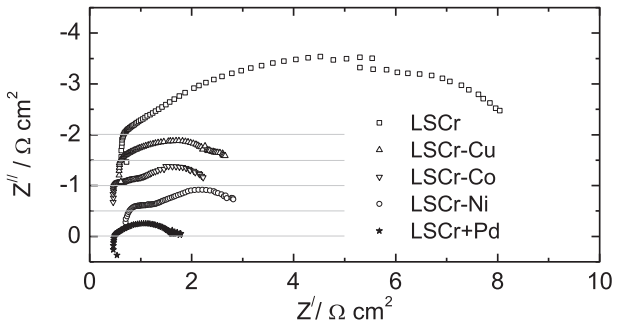


**Fig. 7.** Open circuit voltage Cole–Cole plots for cells with 45 wt% transition-metal doped LSCr calcined at 1473 K. The transition metal dopants are indicated in the figure. For one cell undoped LSCr was used a Pd (0.5 wt%) catalyst was added by infiltration. Operating conditions: 973 K in humidified $H_2$ (3% $H_2O$). Cathodes were exposed to stagnant, ambient air.

**Table 1**
Carbon deposition comparison.

| Carbon formation after dry $CH_4$ exposure (800 °C, 4 h) | |
|---|---|
| Infiltrated materials | % Weight gain |
| Ceria-Co [25] | >100 |
| $Ce_{0.9}Sr_{0.1}Co_{0.1}VO_4$ [8] | 12 |
| $La_{0.8}Sr_{0.2}Cr_{0.9}Co_{0.1}O_3$ | <1 |

however, if added metal catalysts, which are needed to obtain adequate oxidation activity, still catalyze the formation of deactivating carbon filaments. Previous studies of carbon filament formation on transition metal catalysts suggest that this process is dependent on the size of the metal nanoparticles, with particles between 10 and 30 nm being the most active [30,31]. In light of this, we also investigated the hydrocarbon stability of the metal particles exsolved from transition-metal doped LSCr, since the XRD results suggest that they are somewhat smaller. This was done by measuring the weight gain that occurred upon exposing a reduced YSZ slab infiltrated with $La_{0.8}Sr_{0.1}Co_{0.1}O_3$ to dry methane for 4 h at 1073 K. As shown in Table 1, the % weight gain was <1% indicating that carbon deposition or filament formation was negligible. Note that this is in contrast to what has been reported previously for Co particles on a ceria support [32] and for Co particles formed by exsolution from $Ce_{0.9}Sr_{0.1}Co_{0.1}VO_4$ [15], where significantly higher weight gains were observed for similar conditions. While additional study is needed to fully explore the hydrocarbon stability of the reduced, transition-metal doped LSCr family of perovskites, these results suggest that they may be relatively stable in hydrocarbon fuels possibly due to the small size of the metal particles that are formed.

## 4. Conclusions

The results obtained in this study demonstrate that LSCr/YSZ composites produced by infiltration of LSCr into a preformed, porous YSZ scaffold have electronic conductivity under reducing conditions (~1 S $cm^{-1}$ at 700 °C) that is an order of magnitude higher than that of LSCM/YSZ composites. Despite the high conductivity, LSCr/YSZ composite SOFC anodes exhibited somewhat lower performance than those based on LSCM/YSZ. This appears to be due to differences in the microstructures of the infiltrated LSCr and LSCM films. Upon reduction the LSCM forms a highly textured, porous, interconnected film with a relatively high surface area and high concentration of TPB sites. In contrast the LSCr forms large (~0.5 μm diameter), poorly connected particles resulting in a much lower surface area and lower electrochemical activity.

Studies of the enhancement of the catalytic properties of LSCr demonstrated that catalytic metal nanoparticles could be produced by exsolution of dopant transition metal ions (Cu, Co, and Ni) from the LSCr lattice. These metal nanoparticle catalysts significantly enhanced the overall performance of LSCr/YSZ composite SOFC anodes. Exsolved Co nanoparticles were also found to have low activity for the formation of carbon deposits when exposed to $CH_4$ at elevated temperatures, possibly due to the small metal particle size. This result is encouraging and suggests that exsolution from a perovskite lattice may be useful method to produce hydrocarbon-stable metal catalysts for SOFC anodes.

## Acknowledgments

The authors would like to thank the U.S. National Science Foundation for financial support for this research project (grant no. DMR-1210388).

## References


[1] S.W. Tao, J.T.S. Irvine, Nat. Mater. 2 (2003) 320–323.
[2] G. Kim, G. Corre, J.T.S. Irvine, J.M. Vohs, R.J. Gorte, Electrochem. Solid-State Lett. 11 (2008) B16–B19.
[3] G. Kim, S. Lee, J.Y. Shin, G. Corre, J.T.S. Irvine, J.M. Vohs, R.J. Gorte, Electrochem. Solid-State Lett. 12 (2009) B48–B52.
[4] J.S. Park, I.D. Hasson, M.D. Gross, C. Chen, J.M. Vohs, R.J. Gorte, J. Power Sources 196 (2011) 7488–7494.
[5] G. Corre, G. Kim, M. Cassidy, J.M. Vohs, R.J. Gorte, J.T.S. Irvine, Chem. Mater. 21 (2009) 1077–1084.
[6] J.-S. Kim, S. Lee, R.J. Gorte, J.M. Vohs, J. Electrochem. Soc. 158 (2011) B79–B83.
[7] S. Lee, G. Kim, J.M. Vohs, R.J. Gorte, J. Electrochem. Soc. 155 (2008) B1179–B1183.
[8] Z. Zhan, D.M. Bierschenk, J.S. Cronin, S.A. Barnett, Energy Environ. Sci. 4 (2011) 3951–3954.
[9] S.P. Jiang, L. Liu, K.P. Ong, P. Wu, J. Li, J. Pu, J. Power Sources 176 (2008) 82–89.
[10] J.W. Fergus, Solid State Ionics 171 (2004) 1–15.
[11] J. Mizusaki, S. Yamauchi, K. Fueki, A. Ishikawa, Solid State Ionics 12 (1984) 119–124.
[12] B.D. Madsen, W. Kobsiriphat, Y. Wang, L.D. Marks, S.A. Barnett, J. Power Sources 166 (2007) 64–67.
[13] W. Kobsiriphat, B.D. Madsen, Y. Wang, M. Shah, L.D. Marks, S.A. Barnett, J. Electrochem. Soc. 157 (2010) B279–B284.
[14] D.M. Bierschenk, E. Potter-Nelson, C. Hoel, Y. Liao, L.D. Marks, K.R. Poeppelmeier, S.A. Barnett, J. Power Sources 196 (2011) 3089–3094.
[15] L. Adijanto, V.B. Padmanabhan, R.J. Gorte, J.M. Vohs, J. Electrochem. Soc. 159 (2012) F751–F756.
[16] S.-H. Cui, J.-H. Li, X.-W. Zhou, G.-Y. Wang, J.-L. Luo, K.T. Chuang, Y. Bai, L.-J. Qiao, J. Mater. Chem. A 1 (2013) 9689–9696.
[17] D. Neagu, G. Tsekouras, D.N. Miller, H. Ménard, J.T.S. Irvine, Nat. Chem. 5 (2013) 916–923.
[18] A.K. Patra, Sathi Nair, P.U. Sastry, A.K. Tyagi, J. Alloys. Compd. 475 (2009) 614–618.
[19] R. Kungas, J.-S. Kim, J.M. Vohs, R.J. Gorte, J. Am. Ceram. Soc. 94 (2011) 2220–2224.
[20] H. He, Y. Huang, J. Regal, M. Boaro, J.M. Vohs, R.J. Gorte, J. Am. Ceram. Soc. 87 (2004) 331–336.
[21] Y. Huang, J.M. Vohs, R.J. Gorte, J. Electrochem. Soc. 151 (2004) A646–A651.
[22] M. Boaro, J.M. Vohs, R.J. Gorte, J. Am. Ceram. Soc. 86 (2003) 395–400.
[23] A.C. Larson, R.B. Von Dreele, Los Alamos National Laboratory Report LAUR 86-748, 2000.
[24] B.H. Toby, J. Appl. Cryst. 34 (2001) 210–213.
[25] I. Yasuda, M. Hishinuma, Solid State Ionics 80 (1995) 141–150.
[26] K.-J. Yoon, C.N. Cramer, E.C. Thomsen, C.A. Coyle, G.W. Coffey, O.A. Marina, J. Electrochem. Soc. 157 (2010) B856–B861.
[27] Y.-P. Fu, H.-C. Wang, J. Ouyang, Int. J. Hydrogen Energy 36 (2011) 13073–13082.
[28] W. Wang, M.D. Gross, J.M. Vohs, R.J. Gorte, J. Electrochem. Soc. 154 (2007) B439–B445.
[29] C. Arrivé, T. Delahaye, O. Joubert, G. Gauthier, J. Power Sources 223 (2013) 341–348.
[30] L.B. Avdeeva, D.I. Kochubey, Sh.K. Shaikhutdinov, Appl. Catal. A 177 (1999) 43–51.
[31] S. Takenaka, M. Ishida, M. Serizawa, E. Tanabe, K. Otsuka, J. Phys. Chem. B 108 (2004) 11464–11472.
[32] S.-I. Lee, K. Ahn, J.M. Vohs, R.J. Gorte, Electrochem. Solid-State Lett. 8 (2005) A48–A51.